Revista de Eletrônica de Potência - Sobraep, vol. 12, no. 2, julho de 2007, pp. 113-120. ISSN 1414-8862

PHOTOVOLTAIC SYSTEM FOR SUPPLYING PUBLIC LIGHTING AS PEAK DEMAND SHAVING

Edilson Mineiro Sá Jr.[1], Sergio Daher[2], Fernando L. M. Antunes[3], Cícero M. T. Cruz[4], Kátia M. Silva[5] and A. Ribamar Figueira[6]

Energy Processing and Control Group, Electrical Engineering Department, Federal University of Ceará
Caixa Postal 6001 – Campus of Pici – 60.455-760 – Fortaleza – CE – Brazil
[1]edilson@dee.ufc.br, [2]sdaher@secrel.com.br, [3]fantunes@dee.ufc.br, [4]cicero@dee.ufc.br, [5]katia@coelce.com.br, [6]aribamar@coelce.com.br

***Abstract* – This paper describes the design and implementation of a grid connected photovoltaic system aimed to supply energy to the public lighting during the time of high peak demand of the grid. The system is made of two main parts: the solar energy storage unit and the lighting unit. The energy storage unit is composed by a PV panel operating at its maximum power point (MPP) and a battery charger. The lighting unit is composed by an electronic reactor (ballast) for high pressure sodium (HPS) lamp, that operates with zero-voltage switching (ZVS), and a flyback converter to boost the battery voltage to the level required by the electronic reactor. The interconnection between the electric grid and the proposed system is made by a rectifier with a power factor correction (PFC) stage connected in dc link of the electronic reactor. A microcontroller determines if the battery bank or the grid supplies the lighting unit. Simulation and experimental results for the proposed system supplying a 70W HPS lamp are presented. A prototype, which is in continuous operation for more than two years in the field, is also presented.**

Keywords – PV systems, ballast, charge controller and microcontroller.

I. INTRODUCTION

As PV system prices have continued declined [1], interest in the technical and economic feasibility of using photovoltaic systems in peak-shaving applications on commercial buildings has grown. In a variety of projects, government agencies are demonstrating the economic and environmental value of using distributed energy resources to provide reliable electricity. These projects show how renewable distributed energy resources (DER) can be effectively integrated into utility power grids to provide added power during peak demand.

The public lighting can impose to the electric distribution system a high peak demand. At dusk, most of the commercial and industrial loads are still in operation and houses and public lights are turning on, therefore the electric distribution system is prone to be at high power demand.

Many PV systems have been proposed for public lighting in autonomous installations [2, 3, 4] as the unique energy source, some others have been proposed for grid connected operation as part of distributed generation [5]. A PV system can be used to promote a shaving on the demand of the distribution network caused by the public lighting. For such use, solar energy should be stored at day light and supplied to the grid or alternatively to the public lighting at evenings in time of high peak demand. This new conception allows a reduction in the size of the PV panel and of the battery bank, consequently a decrease of the system cost, which is an advantage for urban areas use.

This paper describes the design and prototype implementation of a grid connected photovoltaic system to supply energy to a 70W high pressure sodium (HPS) lamp for public lighting during the time of high peak demand. During the day, the solar energy is captured by a photovoltaic panel and stored in lead acid batteries through a charge controller. Just after the sun has set the battery bank supplies a HPS lamp during the period of high peak demand. After then the lamp is supplied by the electric grid.

The system, which block diagram is shown in Figure 1, is made by an electronic reactor (ballast), that operates with zero volt switching (ZVS), a power factor correction (PFC) stage, a flyback converter to boost the battery voltage to the level required by the ballast, a charger controller to charge the battery bank and the PV panel which operates at maximum power point. The control strategy is provided by an AVR microcontroller AT90S8535 of Atmel™. The system uses the photovoltaic panel also as a light sensor. When there is no sun light the flyback dc-dc converter goes into operation. The electric grid is disconnected from the ballast and the battery bank supplies the ballast through the dc-dc converter, which output is connected directly in the dc link of the electronic ballast. The half bridge circuit of the electronic ballast and the igniter circuit turn the lamp on. After the period of high peak demand the flyback converter is turned off, and the energy for the lamp comes from the grid.

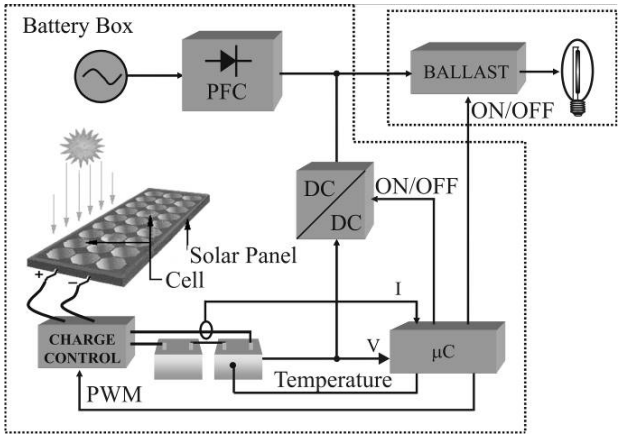

Fig. 1–Diagram in blocks of the developed system.

II. SIZING OF THE PHOTOVOLTAIC PANEL AND BATTERY BANK

In order to size photovoltaic panel and the battery bank an important information is the duration of the period of high peak demand. Information from electric energy distribution utilities state that the period of high peak demand starts at dusk and last for about 2.5 hours, for that is the time when the industrial and commercial loads are been supplied by the distribution system and lighting from houses and streets goes into operation.

The proposed system is mathematically modeled according to [6]. The average power that should be supplied by the battery bank during the system operation is defined by the equation 1.

$$P_{Bat} = \frac{P_{out}}{\eta} \quad (1)$$

P_{Bat} → Average power supplied by the battery bank.
η → System efficiency.
P_{out} → Power drained by the load.

The consumption of the system in amperes hour per day (Ah/day) is defined by the equation 2.

$$Ah_L = \frac{P_{Bat} \cdot t_{func}}{V_{DC}} \quad (2)$$

Ah_L → Diary consumption of the load (Ah).
t_{func} → Time of operation of the load in a day (h).
V_{DC} → Voltage of the battery link (12V, 24V, etc.).

The average capacity of electrical energy production, in amperes hour per day of a photovoltaic module of 12V is given by equation 3.

$$Ah_d = \frac{I_{Rs} \cdot R_{med}}{R_s} \quad (3)$$

Ah_d → Energy supplied by the photovoltaic module per day (Ah).
R_{med} → Diary radiation energy average at the installation place (Wh/m^2).
R_S → Solar radiation intensity (1000 W/m^2).
I_{RS} → Current supplied by the 12V module for radiation R_s (A).

The minimum number of photovoltaic modules necessary for the specified energy consumption is given by equation 4.

$$Np = \frac{Ah_L \cdot V_{DC}}{Ah_d \cdot 12} \quad (4)$$

Ah_L → Capacity of daily consumption of the load (Ah).

The energy storage capacity of the battery bank necessary for operation of the system is given by equation 5.

$$C_{bat} = \frac{Ah_L \cdot d \cdot V_{DC}}{Dc \cdot V_{bat}} \quad (5)$$

C_{bat} → Total energy storage capacity of the battery bank.
d → Autonomy days.
V_{DC} → Voltage of the batteries link.
Dc → Discharge depth.
V_{bat} → Individual battery voltage.

The individual energy storage capacity of a battery is determined by dividing the total energy storage capacity of the bank per number of the batteries in series. The relation current versus time (Ah) usually specifies the battery energy capacity. This value is shown in all batteries and is based on a 20 hours of uninterrupted operation.

For daily solar radiation average energy of 5500Wh/m^2 which is the value for Fortaleza-Ceará-Brazil, 2.5 hours of operation, system efficiency of 80%, 70W HPS lamp, 30% depth of discharge and battery bank voltage of 24V, two 45Ah stationary batteries and one 75Wp photovoltaic module are required.

III. THE BATTERY BANK CHARGER

To maximize the power output from the photovoltaic panel, maximum power point tracker (MPPT) algorithms should be used. For the system design, it is necessary a model for the photovoltaic module [7]. This model is shown in Figure 2. R_s is the resistance of the metallic contacts with the load and R_p the equivalent resistance of the pn junction of a photovoltaic cell.

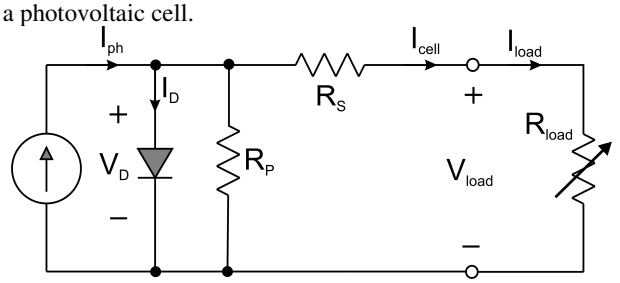

Fig. 2 - The electric model for a photovoltaic cell with load.

The electric model, for the photovoltaic cell can be represented mathematically by equation 6.

$$I_{cell} = I_{ph} - I_0 \cdot \left(e^{\frac{q}{A \cdot k \cdot T}(V_{load} + I_{cell} \cdot R_s)} - 1 \right) - \frac{V_{load} + I_{cell} \cdot R_s}{R_p} \quad (6)$$

I_{cell} → Cell output current (in A).
I_{ph} → Light-generated current (in A).
I_0 → Cell reverse saturation current or dark current (in A).
q → Electronic charge ($1.6 \cdot 10^{-19}$ C).
V_{load} → Cell output voltage (in V).
A → Ideality constants.
K → Boltzmann`s constant ($8.65 \cdot 10^{-5}$ eV/K).
T → Cell temperature (in K).

An association of cells forms the photovoltaic module and its possible circuit representation is showed in Figure 3 [8]. Where R_{SM} is the equivalent series resistance, R_{PM} the equivalent parallel resistance of the module, NP number of cells in parallel, NS number of cells in series and I_{phM} the current supplied by the current source of the module.

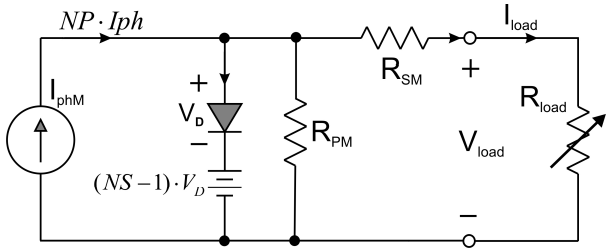

Fig. 3 - The electric model for a photovoltaic module with load.

The manufacturer's manual supplies the maximum current which is equivalent the module short circuit current (I_{short}), maximum voltage which is the module open circuit voltage (V_{open}), the rated current which is the MPP current (I_{MPP}) and rated voltage equivalent the MPP voltage (V_{MPP}). These values are based on 1000 W/m^2 of the solar radiation intensity and temperature of 25°C. Table I shows the values for the chosen PV module.

TABLE I
Electric characteristics of the SP75 Siemens module

75W SP75 module (Siemens)	
Short circuit current (I_{short})	4.8 A
Open circuit voltage (V_{open})	21.7 V
Rated current (I_{MPP})	4.4 A
Rated voltage (V_{MPP})	17 V

In the maximum power point, considering that R_{PM} is much larger than R_{SM}, the current source of the photovoltaic module (I_{phM}) can be approximated to the maximum current (I_{short}) and the polarization diode voltage (V_D) to the open circuit voltage (V_{open}). The equivalent circuit is shown in the Figure 4.

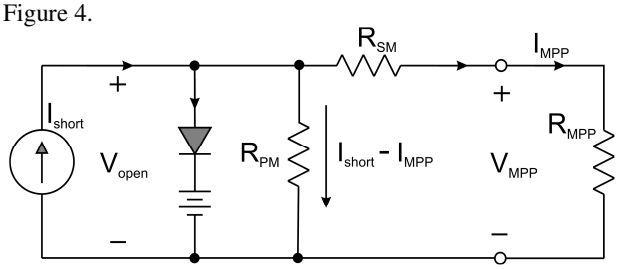

Fig. 4 - Equivalent circuit of the module in the maximum power point.

With the circuit showed in Figure 4, the R_{SM} value can be obtained trough the equation 7.

$$R_{SM} = \frac{V_{open} - V_{MPP}}{I_{MPP}} \Rightarrow R_{SM} = \frac{21.7 - 17}{4.4} \cong 1.068\ \Omega \quad (7)$$

Similarly, the R_{PM} value can be founded by the equation 8.

$$R_{PM} = \frac{V_{open}}{I_{short} - I_{MPP}} \Rightarrow R_{PM} = \frac{21.7}{4.8 - 4.4} \cong 54.25\ \Omega \quad (8)$$

Figure 5 and Figure 6 show, respectively, the simulation results for the IxV and the PxV characteristic of a PV module using the circuit proposed in Figure 3, with R_{PM} and R_{SM} found. It is interesting to note the dual behavior of a PV module: It presents a current source behavior for voltages below the MPP voltage and a voltage source characteristic for voltages above the MPP voltage of the module.

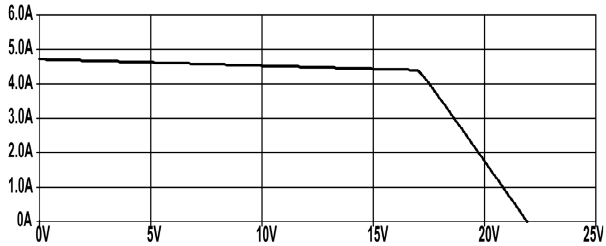

Fig. 5 – The IxV curves of the photovoltaic module obtained by simulation.

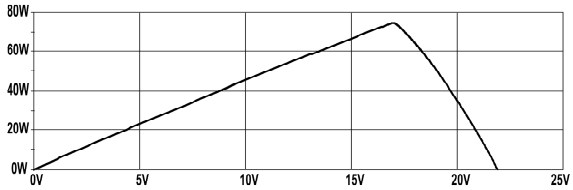

Fig. 6 – Simulated PxV Curve of the photovoltaic module.

Through the analyze of Figure 5 and Figure 6 it can be observed that the simulated characteristics are similar to the real one of the photovoltaic module, as showed in the Figure 7. These results validate the mathematical model here used.

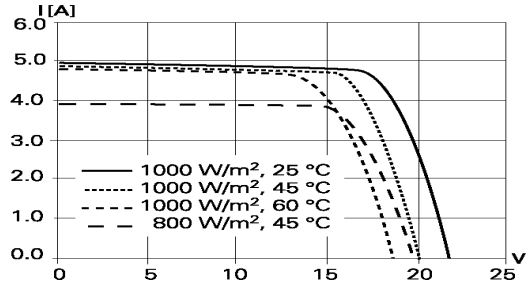

Fig. 7 - The IxV curves of the photovoltaic module obtained from the manufacturer's manual.

To reduce the current value of the converter and minimize the switches conduction losses, it has been chosen 24V as the battery bank dc link voltage. However, this specification leads to the use of a step-up converter to MPPT. The boost converter has been chosen for the application.

The photovoltaic module operating around the maximum power point, may behave as current source or voltage source. The use of a capacitor (Ce) in parallel with the photovoltaic panel, as shown in the Figure 8, ensures a voltage source characteristic at the input of the boost dc-dc converter. Another advantage of the utilization of a capacitor at the boost converter input is a voltage ripple reduction across the photovoltaic panel. This is useful for the maximum power point tracking.

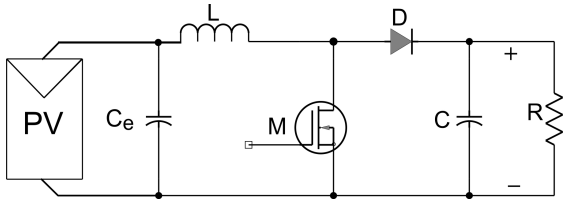

Fig. 8 – The boost converter connected with photovoltaic module and input capacitor.

Considering that current ripple through the inductance is supplied by the capacitor (Ce) in parallel with the panel, equation 9 can be established.

$$\frac{1}{2} Ce(V_{MAX}^2 - V_{MIN}^2) = \frac{1}{2} L(I_{MAX}^2 - I_{MIN}^2) \quad (9)$$

Ce →Capacitor in parallel with the panel.
V_{MAX} →Maximum voltage across the boost converter input.
V_{MIN} →Minimum voltage across the boost converter input.
L →Boost inductance.
I_{MAX} →Maximum current throughout the boost inductance.
I_{MIN} →Minimum current throughout the boost inductance.

Taking into account the converter rated current and its maximum ripple, the value of the capacitor can be determined by equation 10.

$$Ce = \frac{L.I_{RATED}.\Delta I}{V_{RATED}.\Delta V} \quad (10)$$

ΔI → Current ripple of the boost inductance current.
I_{RATED} → Rated current of the boost converter.
V_{RATED} → Rated voltage of the boost converter.
ΔV → Voltage ripple of the boost converter input voltage.

The simulation circuit for the battery charger unit is shown in Figure 9. The boost inductance L1 is designed to operate in continuous conduction.

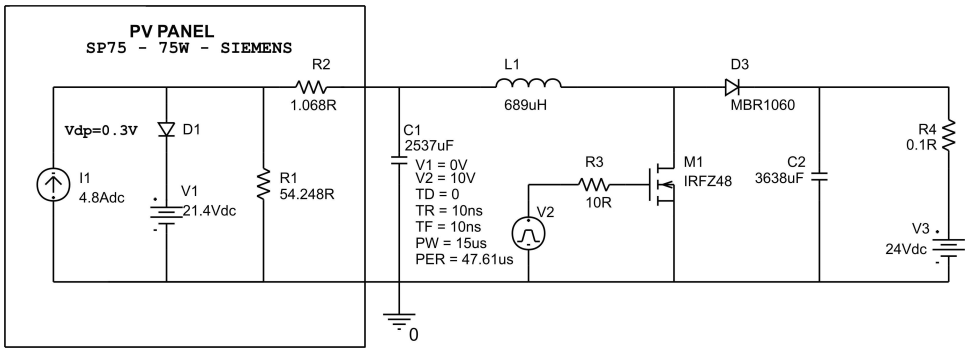

Fig. 9 – The charge controller with the Siemens™ SP75 photovoltaic panel.

The capacitor C1, which is equivalent to capacitor Ce in Figure 8, has been determined by equation 10. The resistance R1, represents R_{PM}, and R2 represents R_{SM}. These values were obtained from the data sheet supplied by the module manufacturer. The resistor R4 represents the internal battery resistance and the shunt resistor used as current sensor.

For a short time interval the battery voltage can be considered as constant, so, the MPP can be obtained by tracking the maximum charge current into the battery [9, 10, 11]. This methodology is different from the traditional perturb and observe algorithm that determines the maximum power point through the multiplication of the current by the voltage in the panel [12, 13]. Figure 10 shows the maximum power point tracking algorithm implemented in the microcontroller.

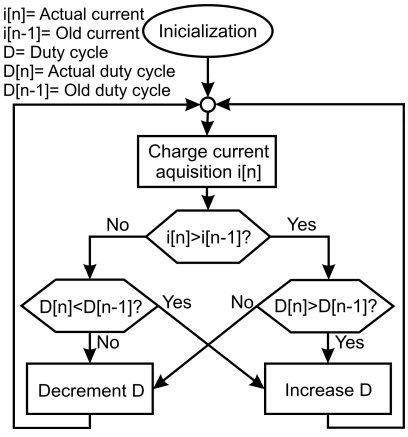

Fig. 10 – MPPT algorithm implemented in the microcontroller.

The boost operation is function of the battery bank voltage (V_{bat}). The charge control algorithm operates according to Figure 11. If the battery bank voltage is below to 14 V the boost converter is off, but the battery charge is carried out through the boost diode (diode D3 in Figure 9). The MPPT goes into action for a battery bank voltage between 14V and 27.6V. For voltages between 27.6V and 28.8V the boost converter duty cycle is fixed in 5%. This duty cycle guarantees the complete battery charge and minimizes the electrolyte loss in the batteries [9]. For voltages above 28.8V the battery is completely charged and the converter is turned off.

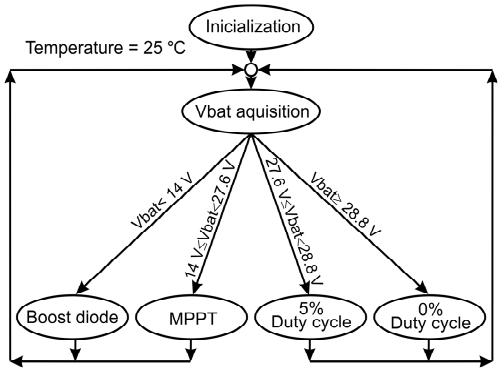

Fig. 11 – Routines for charge the batteries.

The reference voltage used to determine the starting operation of the charge subroutines change with temperature of the batteries. For the battery voltage correction equation 11 is used.

$$V_{correc} = V_{25°C} - \left[\alpha \cdot \left(T_{mes} - T_{cons}\right)\right] \quad (11)$$

V_{correc} → Individual battery voltage corrected.
$V_{25°C}$ → Individual battery voltage in 25 °C.
T_{mes} → Battery temperature measured (in °C).
T_{cons} → Standard temperature (25 °C).
α → Multiplication factor (0.33 V·°C^{-1}).

For stationary battery used in photovoltaic systems the current cannot be larger than a tenth of the battery capacity for overcurrent reduces the battery life time or can damage it. However for systems with high autonomy operation the

size of the battery bank should have a high capacity, consequently, in these systems, the charge current is far below the battery bank current.

The PV module output voltage is showed in Figure 12. It can be observed that the charge controller makes the PV module to operate at the MPP voltage. Other important characteristic that can be observed is the absence of voltage ripple at the PV panel output voltage, making it easier to track the MPP.

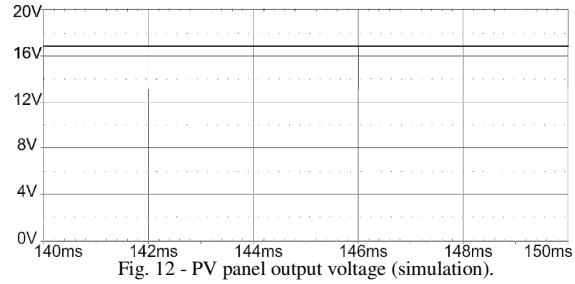

Fig. 12 - PV panel output voltage (simulation).

IV. DC/DC CONVERTER AND GRID CONNECTION

The converter used to step up battery bank voltage as well as to promote the galvanic isolation between the PV panel and the grid was a flyback converter. This converter increases the battery bank voltage (20V to 28V) to dc link voltage (311V) required by the electronic reactor (ballast). Figure 13 shows the block diagram of the circuit used to supply the HPS lamp.

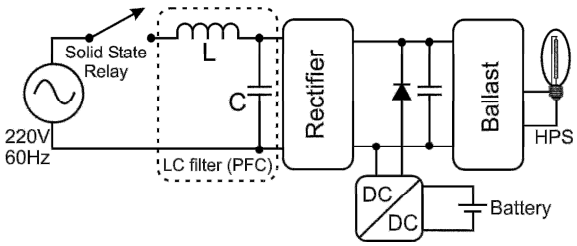

Fig. 13 - HPS lamp supply systems.

The power factor correction (PFC) used was made by a LC filter, shown in Figure 13. This filter is bulky but it is simple and very robust to voltage variations of the grid. However, the use of LC filters with resonance frequency near of the electric grid frequency, the grid should be disconnected during the flyback operation (dc-dc converter in Figure 13). A solid state relay, a TRIAC with RC snubber [14], was used to disconnect the grid. The flyback should be on before the grid disconnection, for the lamp not to turn off.

V. ELECTRONIC REACTOR

The electronic reactor requires a very careful design, because during the ignition process, voltages in the order of 3kV are generated in the HPS lamp. However there are some advantages in using an electronic reactor due to its compactness, the ignition circuit is part of the reactor and the lamp flicker is attenuated due to the high frequency operation of the lamp.

The electronic reactor inverter is a half bridge structure, which simplified model can be seen in Figure 14. The commutation frequency of the switches has been chosen as 33kHz, to avoid the possibility of acoustic resonance in the HPS SON 70W E (Phillips) lamp [15]. The circuit tank, formed by L_R and C_R, has been designed for the ZVS operation of the switches [16].

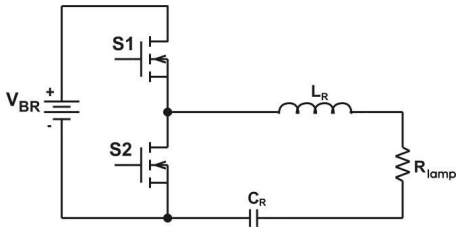

Fig. 14 - The simplified half bridge model for HPS lamp.

The HPS lamp is represented by a resistance because of the high frequency operation of the switches, the gas within the lamp stays ionized even during the zero crossing of the current.

The electronic reactor presents four operating stages.

The first stage, shown in Figure 15, starts when D1 goes into conduction. The energy stored in L_R goes back to the supply. In this stage the lamp current is negative and decrease to zero.

The second stage starts with the conduction of S1, the lamp current is positive and increases up to the maximum value. This stage is shown in Figure 15.b.

The third stage is similar to the first one but the current is positive. This stage is shown in Figure 15.c.

The fourth stage, shown in Figure 15.d, starts with the conduction of S2. The current increase towards the negative direction until D1 is forward biased, starting back the fist stage.

Details about the design of L_R and C_R are found in [17].

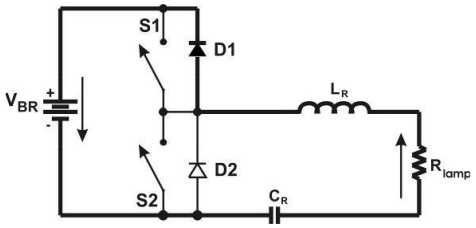

Fig.15.a - First stage.

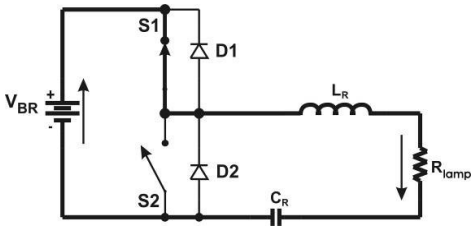

Fig.15.b - Second stage.

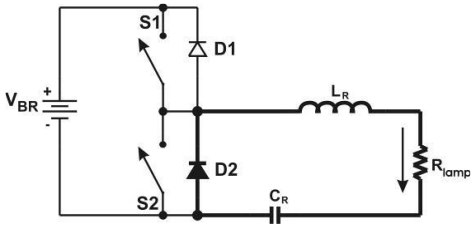

Fig.15.c - Third stage.

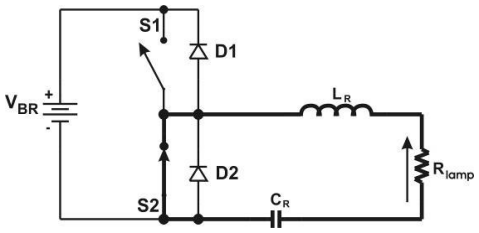

Fig.15.d – Fourth stage.

VI. EXPERIMENTAL RESULTS

The charge controller input voltage and current are shown in Figure 16, for fixed duty cycle. No voltage or current ripple is observed in the photovoltaic panel. For the experimental results a PV module which presented characteristcis equal to those presented by the manufacturer has been chosen.

The battery charging current can be seen in Figure 17. The current ripple is smoothed by the capacitor connected at the boost output stage.

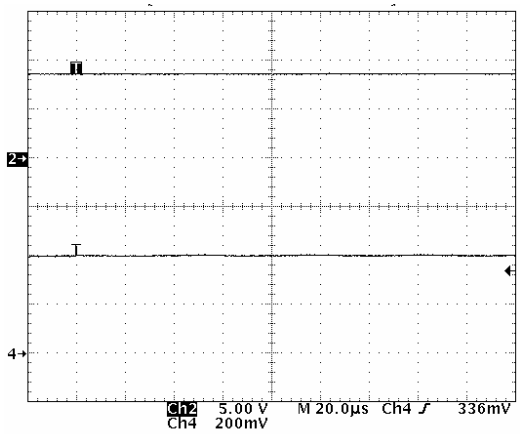

Fig. 16 – Photovoltaic module voltage, channel 2 (5V/div), and current, channel 4 (2A/div).

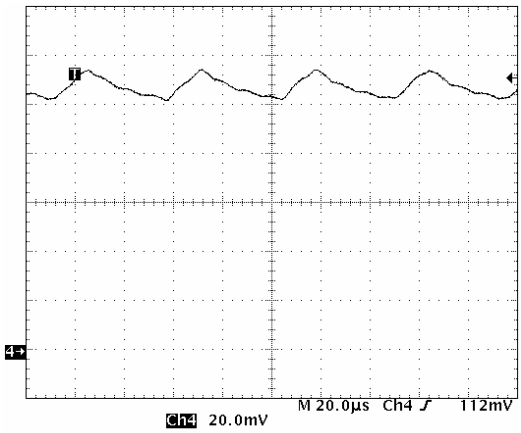

Fig. 17 – Battery charge current (200mA/div).

The HPS lamp voltage and current can be observed in Figure 18.

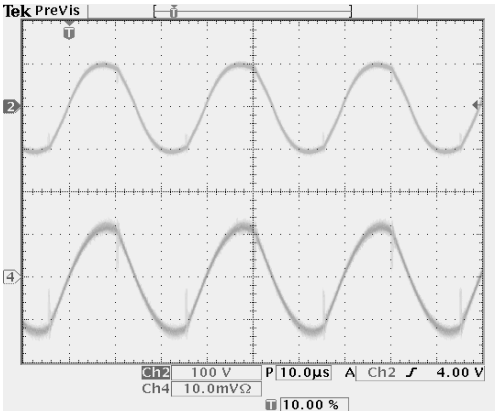

Fig. 18 – Lamp voltage, channel 2 (50V/div), and current, channel 4 (1A/div).

Figure 19 shows the picture of the electronic reactor implemented in the laboratory.

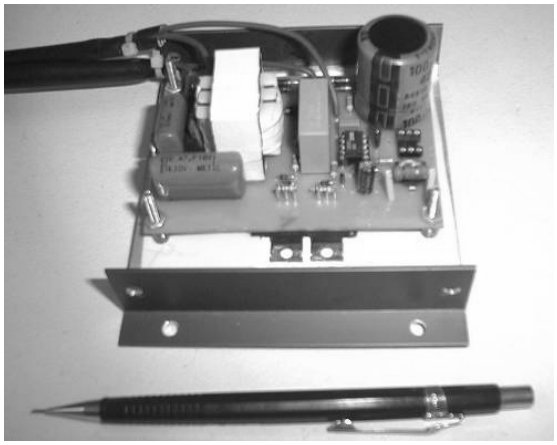

Fig. 19 – Electronic reactor picture.

Figure 20 shows a picture of the implemented charge controller.

Fig. 20 – Picture of the charge controller in operation.

Figure 21 shows the implemented electronic reactor picture and the HPS lamp at the ignition instant.

Fig. 21 – Ignition moment of the lamp.

Figure 22 shows a picture of the prototype in operation in the field. It is in continuous operation for almost three years, and up to now no miss operation or component failure has been presented, even the battery bank.

As far as the economical advantage of this system, considering the cost of the energy at time of high peak demand, the payback of an unit would last ten years [17]. However, the modular characteristic of the system allows its use as an autonomous energy supply system as well. When used in places where the grid extension presents high cost, the autonomous operation of the system here proposed is already competitive.

Fig. 22 – Developed prototype in operation in the field.

VII. CONCLUSIONS

This paper presented the design and prototype implementation of a grid connected photovoltaic system to supply energy to the public lighting for two hours and a half aiming peak demand shaving.

A computational model to analyse the operation of the PV panel and the charge controller has also been presented. The charger controller used was a dc-dc boost converter and lead the PV panel to operate at the MMP. The half-bridge circuit used in the electronic reactor presents the advantage of having incorporated lamp igniter. The switching frequency of the ballast was chosen as 33kHz to avoid acoustic resonance which otherwise could lead the lamp to explode. The ZVS commutation techniques used in the electronic ballast made it possible to reduce losses and consequently an increment in the circuit efficiency. Another positive point of this technique is the EMI reduction.

The efficiency of the charge controller reached 95%, the flyback converter 92% and the electronic ballast 89%.

This new conception allows a reduction in the size of the PV panel and of the battery bank, consequently a decrease of the system cost, which is an advantage for application in urban areas. Another advantage that can be pointed out is that the system, not the public grid, supplies energy to the HPS lamp at the time of peak demand, when the price of the electricity from the grid is higher. This brings a reduction on the payback time of the proposed system.

The prototype is in continuous operation for almost three years, and up to now no missoperation or component failure has been observed.

VIII. ACKNOWLEDGEMENT

Research carried out with financial support of COELCE, the electricity distribution utility of Ceará, within the Research and Development Program of the company.

IX. REFERENCES

[1] M. Staffhorst, “The Way to Competitiveness of PV – An experience Curve and Break-even Analysis”, *PhD Thesis Universität-Kassel, 2006 ISBN 13:978-3-89958-241-3 Kassel University Press GmbH.*

[2] S. R. Harrington and T. D. Hund, “Photovoltaic lighting system performance”, *IEEE 25th Photovoltaic Specialists Conference*, May 1996, pp. 1307-1310.

[3] G. Loois, H. de Gooijer, T. van der Weiden and X.Vallvé, “Large scale market introduction of PV public lighting”, *2th Word Conference and Exhibition Photovoltaic Solar Energy Conversion*, July 1998, pp. 3107-3110.

[4] N. N. Franceschetti, E. B. Schonward and M. Godoy Simões, “Solar energy based public area illumination system”, *COBEP*, vol. 1, 1999, pp. 487-492.

[5] S. B. Kjaer, J. K. Pedersen and F. Blaabjerg, “A review of single-phase grid-connected inverters for photovoltaic modules” *IEEE Transactions on Industry Applications*, vol. 41, no. 5, Sept.-Oct. 2005, pp. 1292-1306.

[6] D. C. Martins, M. Mezaroba and I. Barbi, "Treatment of the Solar Energy for a Water Pumping System Using a Current-Fed Parallel Resonant Push-Pull Inverter", *COBEP*, 1999.

[7] C. Hua and C. Shen, "Comparative study of peak power tracking techniques for solar storage system", *Applied Power Electronics Conference and Exposition 1998 - APEC '98*, Conference Proceedings, Thirteenth Annual, vol. 2, 15-19 Feb. 1998, pp. 679-685.

[8] M. Veerachary, T. Senjyu and K. Uezato, "Maximum power point tracking control of IDB converter supplied PV system", *IEE Proc. Electr. Power Appl.*, vol. 148, no. 6, nov. 2001, pp. 494-502.

[9] F. A. Himmelstoss, A. Laimer and A. Brock, "Microcontroller solar battery charge", *2th Word Conference and Exhibition Photovoltaic Solar Energy Conversion*, July 1998, pp. 3127-3130.

[10] E. Koutroulis, K. Kalaitzakis and N. C. Voulgaris, "Development of a microcontroller-based, photovoltaic maximum power point tracking control system", *IEEE Tran. On Power Electronics*, vol. 16, no. 1, Jan. 2001, pp. 46-54.

[11] L. Zhang, A. Al-Amoudi and Yunfei Bai, "Real-time maximum power point tracking for grid-connnected photovoltaic systems", *IEE Conf. Power Eletronics and Variable Speed Drives*, Set. 2000, pp. 124-129.

[12] M. F. Shraif, C. Alonso and A. Martinez, "A simple robust maximum power point control (MPPC) for ground photovoltaic generators", *Intern. Power Eletronics Conf.*, 2000, pp. 158-163.

[13] J. L. Santos, F. Antunes, A. Chehab and C. Cruz, "A maximum power point tracker for PV systems using a high performance boost converter", *Solar Energy July 2006, pp* 760-771.

[14] G. Templeton, "AN1048/D RC Snubber Networks For Thyristor Power Control and Transient Suppression", Application Note, ON Semiconductor, Rev. 2, August 1999.

[15] F. S. Cavalcante, "Reatores eletrônicos para lâmpadas de vapor de sódio de alta pressão de 70W" *Dissertação (Mestrado em Engenharia Elétrica) – INEP/EEL*, UFSC, Florianópolis, Dezembro de 2001.

[16] A. Anderson S. "Sistema eletrônico para lâmpadas de descarga de alta pressão para iluminação de exteriores*", Exame de qualificação*, Santa Catarina, Florianópolis, Julho de 2001.

[17] E. M. Sá Jr. "Sistema Fotovoltaico de Iluminação Pública em Horário de Ponta*", Dissertação (Mestrado em Engenharia Elétrica) – PPGEE*, UFC, Fortaleza, Novembro de 2003.

IX. BIOGRAPHIES

Edilson Mineiro Sá Junior, MSc was born in Fortaleza, Brazil in 1975. He received his BSc. degree from the Federal University of Ceará in Electrical Engineering in 2000 and MSc. Degree in 2004. Currently, he is doctor student in Federal University of Santa Catarina, Florianópolis, Brazil. His main research interests include power supplies, power factor correction techniques, renewable energy systems, ballast (electronic reactor) and illumination with High Power LEDs.

Sérgio Daher. Dr-Ing. B.Sc. degree in Electrical Engineering from Federal University of Paraíba in 1995, MSc. Eng. Degree from Federal University of Ceará in 1997 and Dr degree from University of Kassel, Germany in 2006. His main research interests include power supplies, renewable energy systems and multilevel converters.

Fernando Luis Marcelo Antunes, PhD. B.Sc. degree in Electrical Engineering from Federal University of Ceará-Brazil, in 1978 B.Sc. degree in Business and Administration from the State University of Ceara-Brazil, MSc degree from the University of São Paulo (Brazil), in 1980 and PhD degree from Loughborough University of Technology – United Kingdom (UK) in 1991. He is a lecturer at Federal University of Ceará Brazil, teaching Power Electronics and Electric Machines at graduate and undergraduate levels, and doing research in Power Electronics and its application to renewable energy systems. He coordinates the Energy Processing and Control Group of the DEE of the UFC where research projects are carried out with financial support of research development agencies and public and private companies. He is member of The SOBRAEP, SBA and IEEE.

Cicero Marcos Tavares Cruz, Dr. B.Sc. degree in Electrical Engineering from Federal University of Ceará in 1990, MSc. Eng. Degree in 1993 from University Federal of Santa Catarina and Dr degree from University Federal of Santa Catarina in 2002. He is a lecturer at Federal University of Ceará (Brazil), teaching Power Electronics at graduate and undergraduate levels. His main research interests include power supplies, alternative energy systems, rectifiers, PFC and resonates converters.

Antônio Ribamar Filgueira, Eng. B.Sc. degree in Electrical Engineering from University of Fortaleza – UNIFOR. He works as an engineer of COELCE, the electricity distribution utility of Ceará, Brazil.

Kátia Maria Silva, Eng. B.Sc. degree in Electrical Engineering from Federal University of Paraíba. She works as an engineer of COELCE, the electricity distribution utility of Ceará, Brazil.